Spin-Flow Vibrational Spectroscopy of Molecules with Flexible Spin Density: Electrochemistry, ESR, Cluster and Spin Dynamics, and Bonding in TiSc$_2$N@C$_{80}$

Alexey A. Popov,[†,‡,]* Chuanbao Chen,[§] Shangfeng Yang,[§,]* Ferdinand Lipps,[†] and Lothar Dunsch[†,]*

[†]Leibniz-Institute for Solid State and Materials Research (IFW), Dresden, D-01171 Dresden, Germany, [‡]Department of Chemistry, Moscow State University, Leninskiye Gory, 119992 Moscow, Russia, and [§]Hefei National Laboratory for Physical Sciences at Microscale and Department of Materials Science and Engineering, University of Science and Technology of China (USTC), Hefei 230026, China

ABSTRACT   The recently isolated TiSc$_2$N@C$_{80}$ was used to study the spin state of a Ti^{3+} ion in a mixed metal nitride cluster in a fullerene cage. The electronic state of the new clusterfullerene is characterized starting with the redox behavior of this structure. It differs markedly from that of homometallic nitride clusterfullerenes in giving reversible one-electron transfers even on the cathodic scale. Both oxidation and reduction of TiSc$_2$N@C$_{80}$ occur at the endohedral cluster changing the valence state of Ti from Ti(II) in anion to Ti(IV) in cation. The unpaired electron in TiSc$_2$N@C$_{80}$ is largely fixed at the Ti ion as shown by low temperature ESR measurements. Isotropic g-factor 1.9454 points to the significant spin—orbit coupling with an unquenched orbital momentum of the 3d electron localized on Ti. Measurements with the frozen solution also point to the strong anisotropy of the g-tensor. DFT computations show that the cluster can adopt several nearly isoenergetic configurations. DFT-based Born—Oppenheimer molecular dynamics (BOMD) simulations reveal that, unlike in Sc$_3$N@C$_{80}$, the cluster dynamics in TiSc$_2$N@C$_{80}$ cannot be described as a 3D rotation. The cluster rotates around the Ti—N axis, while the Ti atom oscillates in one position around the pentagon/hexagon edge. Evolution of the spin populations along the BOMD trajectory has shown that the spin distribution in the cluster is very flexible, and both an intracluster and cluster-cage spin flows take place. Fourier transformation of the time dependencies of the spin populations results in the spin-flow vibrational spectra, which reveal the major spin-flow channels. It is shown that the cluster-cage spin flow is selectively coupled to one vibrational mode, thus, pointing to the utility of the clusterfullerene for the molecular spin transport. Spin-flow vibrational spectroscopy is thus shown to be a useful method for characterization of the spin dynamics in radicals with flexible spin density distribution.

KEYWORDS: endohedral fullerenes · nitride clusterfullerene · ESR spectroscopy · molecular dynamics · DFT computations · spin transport · QTAIM · electronic structure

Endohedral fullerenes, that is, fullerenes with atoms or clusters encapsulated in their interior, are known for their special property to stabilize chemical entities that cannot exist outside the carbon cage.[1−5] A majority of the endohedral fullerenes known to date are based on the Group III metals (*i.e.*, Sc, Y, and lanthanides), although Group II and Group IV metallofullerenes are also known. In particular, Ti has a relatively small ionic radius (0.605 Å for Ti^{4+}, 0.67 Å for Ti^{3+})[6] compared to those of other Group III metals (*e.g.*, 0.75 Å for Sc^{3+}), and this might facilitate its encapsulation inside the fullerene. On the other hand, ionization energies of the Ti atom are considerably higher than those of Sc. Until now Ti was reported to form isolatable endohedral metallofullerenes like "Ti$_2$@C$_{80}$" and "Ti$_2$@C$_{84}$".[7,8] As found later, the "Ti$_2$@C$_{80}$" structure turned out to be a Ti$_2$C$_2$ carbide encaged within the C$_{78}$-D$_{3h}$ cage (Ti$_2$C$_2$@C$_{78}$).[9−11] DFT studies suggested the existence of Ti^{4+} cations in the carbide structure trapped in a C$_{78}$$^{6−}$ cage, where two additional negative charges are contributed by the encapsulated C$_2$ carbide unit.[9,10,12] The Ti^{4+} state is also predicted for Ti@C$_{28}$, which was observed in the mass spectra but could not be isolated in appreciable amounts.[13,14] Thus, the data available so far on Ti-based endohedral fullerenes are in line with the fact that Ti is known to exist in the stable ionic state of Ti^{4+}, while the Ti^{3+} is quite reactive and preferably stabilized as a solid.

Metal-nitride cluster fullerenes (NCFs) are a special class of endohedral fullerenes with the trimetallic nitride cluster inside the carbon cage.[3,4,15,16] NCFs have attracted considerable attention in the past decade because of their higher kinetic stability and improved yields compared to the conventional endohedral metallofullerenes. A number of homometallic NCFs have been isolated, including the most studied Sc$_3$N@C$_{2n}$ (2n = 68, 70, 78, 80)[15,17−22] and different M$_3$N@C$_{2n}$ fullerenes (78 ≤ 2n ≤ 88 for M = Y, Gd, Tb, Dy, Ho, Er, Tm, Lu; 80 ≤ 2n ≤ 96 for M = Pr, Nd; 86 ≤ 2n ≤ 96 for M = La, Ce).[23−35] They all exist in the formal electronic configuration of (M$_3$N)$^{6+}$@C$_{2n}$$^{6−}$.[5,12,36−41]
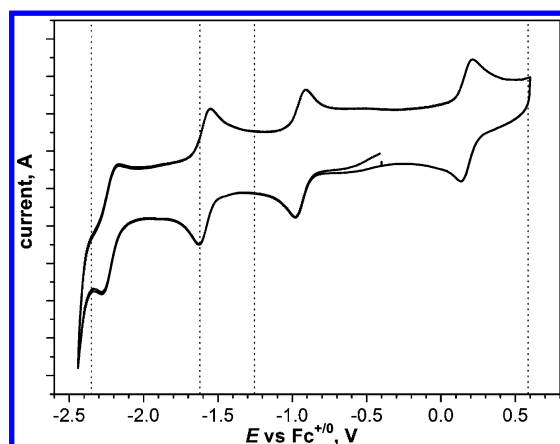
Figure 1. Cyclic voltammetry of TiSc$_2$N@C$_{80}$ measured in *o*-DCB solution (room temperature, TBABF$_4$ as supporting electrolyte) at a scan rate of 20 mV s^{-1}. Dotted vertical bars denote reversible redox potentials of Sc$_3$N@C$_{80}$ (from refs 20 and 51).

Furthermore, mixed metal nitride clusterfullerenes (MMNCFs) such as M$_x$Sc$_{3-x}$N@C$_{80}$ (M = Y, Ce, Nd, Gd, Tb, Dy, Er, Lu)[23,42−48] or Lu$_x$Y$_{3-x}$N@C$_{80}$,[49] have also been isolated. Thus, all of NCFs known to date are limited to the Group III (Sc, Y, and lanthanide) metals. While endohedral metallofullerenes with encaged metals of the Groups II, III, and IV and all the lanthanide metals have been described, the role of Group IV metals in NCFs is still to be followed in detail. Recently we have reported the first synthesis of NCF with a Group IV metal, TiSc$_2$N@C$_{80}$, which was suggested to have a Ti(III) state of titanium.[50] In this work we report an in-depth study of this special NCF by means of cyclic voltammetry, ESR spectroscopy, and DFT computations to reveal the state of Ti in TiSc$_2$N@C$_{80}$ and its influence on the electronic properties, internal dynamics, and chemical bonding in TiSc$_2$N@C$_{80}$ in comparison to Sc$_3$N@C$_{80}$. In the frames of this study we propose a spin-flow vibrational spectroscopy, which combines DFT-based Born−Oppenheimer molecular dynamics with following the spin population to reveal the details of the dynamics of the spin distribution. Although essentially simple, this approach is found to be a powerful tool in the study of the spin dynamics and the spin-transfer channels, which might be of use in the molecular spin transport.

RESULTS AND DISCUSSION

Electrochemistry of TiSc$_2$N@C$_{80}$. Cyclic voltammetry of TiSc$_2$N@C$_{80}$ in solution exhibits one reversible oxidation and three reversible reduction steps at +0.16, −0.94, −1.58, −2.21 V *versus* Fc/Fc$^+$ in 0.1 M TBABF$_4$/ *o*-DCB solution at room temperature and a scan rate of 20 mV s^{-1} (Figure 1). Electrochemical reversibility of the reduction steps of TiSc$_2$N@C$_{80}$ is quite remarkable because reductions of other homometal nitride clusterfullerenes like Sc$_3$N@C$_{80}$ are electrochemically irreversible under the same conditions, and much higher scan rates are required to achieve reversibility.[51] Compared

to Sc$_3$N@C$_{80}$, TiSc$_2$N@C$_{80}$ is easier to oxidize by 0.46 V and easier to reduce by 0.30 V, and hence, the electrochemical gap of TiSc$_2$N@C$_{80}$, 1.10 V, is 0.76 V smaller than that of Sc$_3$N@C$_{80}$ (1.86 V),[20] which is not surprising taking into account the radical nature of TiSc$_2$N@C$_{80}$. At the same time, it is remarkable that the electrochemical gap of TiSc$_2$N@C$_{80}$ is relatively large compared to other radical endohedral metallofullerenes such as Y@C$_{82}$ (0.47 V)[52] or Sc$_3$C$_2$@C$_{80}$ (0.44 V).[53] However, the gap for TiSc$_2$N@C$_{80}$ is 0.34 V smaller than that in CeLu$_2$N@C$_{80}$ (1.40 V), which has an unpaired electron localized on the Ce atom.[54] The difference in the electronic state of TiSc$_2$N@C$_{80}$ as compared to CeLu$_2$N@C$_{80}$ being demonstrated by cyclic voltammetry requires further deep characterization, as given below. We will show that both oxidation and reduction of TiSc$_2$N@C$_{80}$ occur at the endohedral cluster, changing the valence state of Ti from Ti(II) in anion to Ti(III) in the neutral state to Ti(IV) in the cation. While either reduction of the endohedral species (as in Sc$_3$N@C$_{80}$) or their oxidation (as in CeLu$_2$N@C$_{80}$) has been reported,[20,51,54,55] to our knowledge, TiSc$_2$N@C$_{80}$ is the first example of EMF in which the endohedral cluster is electrochemically active in both reduction and oxidation.

ESR Study. The odd number of electrons in TiSc$_2$N@C$_{80}$ suggests that this structure is paramagnetic and, thus, should be ESR active. The measurements of the ESR spectra of the toluene solution at room temperature showed only a very broad ESR line hardly distinguishable from the background. However, lowering the temperature resulted in the narrowing (to a line width of 35 G at 180 K) of a featureless ESR signal with a g-factor of 1.9454 observed in the whole temperature range down to 180 K, the freezing temperature of the solvent (Figure 2a). Further cooling of the solution resulted in a significant change of the ESR spectrum (Figure 2b). At 100 K the signal has two main features and is about 250 G broad, which points to the significant anisotropy of the g-tensor. The latter could not be adequately modeled by the use of three different g$_{xx,yy,zz}$ values, probably because TiSc$_2$N@C$_{80}$ radicals exist in the frozen solution in different environments, including both crystalline and glassy states of toluene. However, the field range covered by the ESR signal suggests that the difference between the largest and the smallest principal moments of the g-tensor should be about 0.08. This as well as the significant shift of the isotropic g-factor value from that of the free electron suggests that the spin density in TiSc$_2$N@C$_{80}$ is to a large extent localized on the Ti atom, and the orbital moment of the *d*-electron is not completely quenched.

In another series of measurements, the fullerene solution was quickly frozen to 4 K, and the ESR spectra were measured then during a stepwise increase of the temperature (Figure 2c). By this method, presumably a glassy state of toluene is obtained, and hence, the ESR spectra are different from those measured during slow
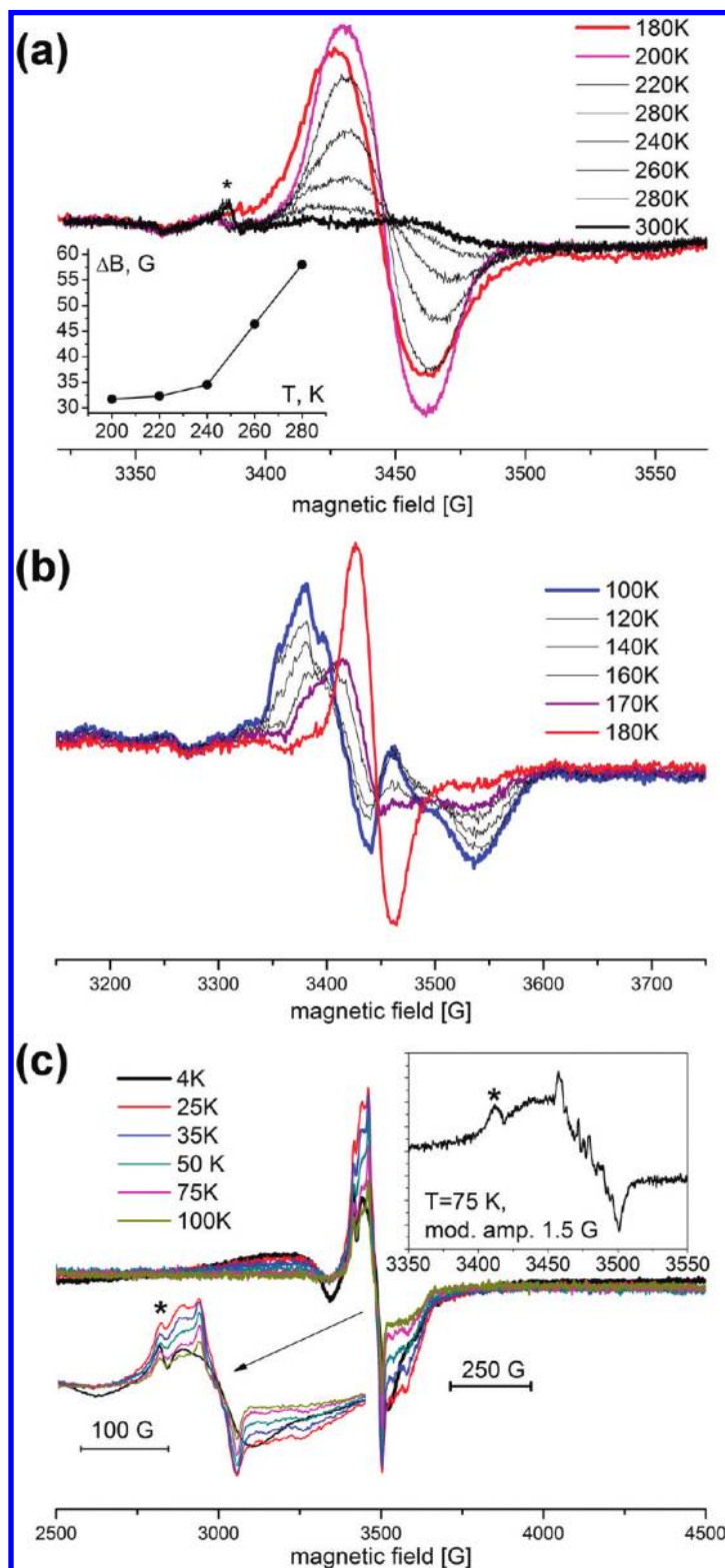
Figure 2. ESR spectra of $TiSc_2N@C_{80}$ in (a) toluene above the melting point of toluene (the inset shows the temperature dependence of the line width); (b) frozen solution obtained by slow cooling; and (c) frozen solution obtained by fast cooling to 4 K and then a slow increase of the temperature (the inset shows the spectrum measured at 75 K with higher resolution). The asterisks in (a) and (c) denote an unidentified impurity. Note that (a) and (b) on the one side and (c) on the other side were measured on different instruments, and hence, the axes are not exactly coinciding.

cooling of the frozen solution. Instead, they are more reminiscent of the spectra measured above the freezing point of toluene overlapped by the much broader

signal. The total line width is about 40 G, and a hyperfine structure due to ^{45}Sc with the hyperfine coupling constant of about 7 G can be seen, although it is still not
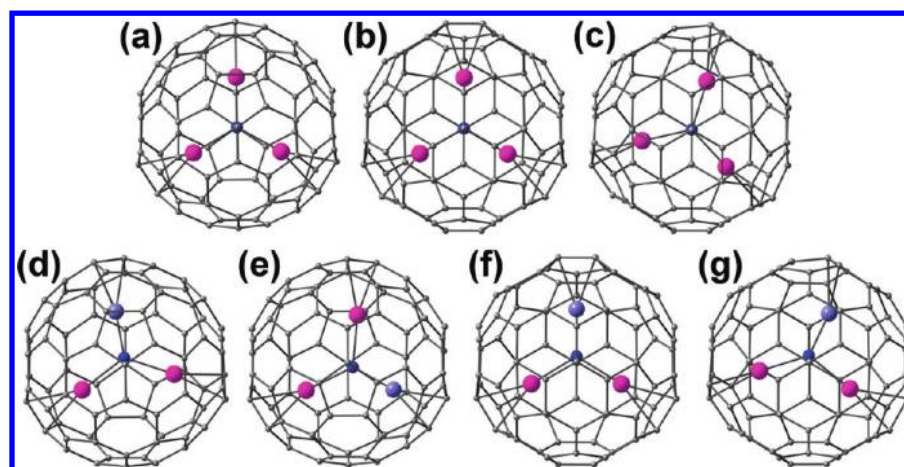
Figure 3. DFT-optimized molecular structures of $Sc_3N@C_{80}$ and $TiSc_2N@C_{80}$ conformers: (a) C_s-$Sc_3N@C_{80}$; (b) C_{3v}-$Sc_3N@C_{80}$; (c) C_3-$Sc_3N@C_{80}$; (d) **1**-$TiSc_2N@C_{80}$; (e)**2**-$TiSc_2N@C_{80}$; (f) **3**-$TiSc_2N@C_{80}$; (g)**4**-$TiSc_2N@C_{80}$. Sc and Ti are shown in magenta and cyan colors, respectively.

sufficiently resolved for the precise determination of the hfc values and their anisotropy.

In summary, VT-ESR measurements show that $TiSc_2N@C_{80}$ is a radical with relatively high anisotropy of the g-tensor. At room temperature the ESR signal is very broad and can hardly be seen, but the low temperature measurements clearly reveal the strong ESR signal. The reasons for the severe broadening of the signal at room temperature are not clear yet and may include the intermediate regime of the rotation of the $TiSc_2N$ cluster (between the slow and fast limits). Unfortunately, attempts to measure the ESR spectra above room temperature in o-DCB solution resulted in the decomposition of the sample.

Molecular Structure of $TiSc_2N@C_{80}$. Numerous studies of $M_3N@C_{80}(I_h)$ reported in the past decade have shown that the M_3N cluster is not tightly fixed in the carbon cage, which results in multiple conformers with close relative energies and small barriers to rotation.[37,56−60] For the $Sc_3N@C_{80}$ (hereafter we will discuss only C_{80}-I_h carbon cage and, hence, its symmetry designation will be omitted), we have shown that the lowest conformer has C_3 symmetry.[12] In this structure, the Sc atoms are facing hexagons but are somewhat displaced toward the pentagon/hexagon (pent/hex hereafter) edge (the structure with all Sc atoms facing the centers of hexagon has D_3 symmetry and is found to be the third order transition state at the PBE/TZ2P level of theory). At the same time, for the $Sc_3N@C_{80}^-$ radical-anion (which is isoelectronic to $TiSc_2N@C_{80}$), the conformer with C_{3v} symmetry was found to be considerably more stable.[12] The second most stable structure both for the neutral and the anionic $Sc_3N@C_{80}$ has a C_s symmetry. Based on these data, in the studies of $TiSc_2N@C_{80}$ in this work, we have started from the three lowest energy conformers of $Sc_3N@C_{80}$ (C_3, C_s, and C_{3v}) and replaced the symmetry inequivalent Sc atoms by Ti (Figure 3). This procedure resulted in four different conformers of $TiSc_2N@C_{80}$ (C_s conformer of $Sc_3N@C_{80}$ gives two different conformers of $TiSc_2N@C_{80}$), which were then fully optimized at the PBE/TZ2P and B3LYP/6-311G* levels of theory. Likewise, we have also optimized the structures of corresponding monoanions and monocations of $TiSc_2N@C_{80}$. Table 1 compares the relative energies of $TiSc_2N@C_{80}$ conformers in different charge states to the conformers of $Sc_3N@C_{80}$ (note the $TiSc_2N@C_{80}^+$ is isoelectronic to $Sc_3N@C_{80}$, while $TiSc_2N@C_{80}^-$ is isoelectronic to $Sc_3N@C_{80}^{2-}$). In the following discussion, we will denote conformers of $Sc_3N@C_{80}$ by their symmetry group, while the conformers of $TiSc_2N@C_{80}$ will be denoted by bold numbers: **1** and **2** denoting the conformers obtained from the C_s conformer of $Sc_3N@C_{80}$, **3** originating from the C_{3v} conformer, and **4** originating from the C_3 conformer (Figure 3).

For the neutral $TiSc_2N@C_{80}$, the conformers **1**, **2**, and **3** have almost the same energies (within 0.8 kJ/mol at the PBE/TZ2P level and within 1.1 kJ/mol at the B3LYP/6-311G* level), while the conformer **4** is considerably less stable. The same trend was found by us earlier for the $Sc_3N@C_{80}^-$ conformers, in which the C_3 structure is also considerably less stable (Table 1).[12] Thus, the fact that $TiSc_2N@C_{80}$ and $Sc_3N@C_{80}^-$ are isoelectronic indeed results in the very similar relative energies of the conformers. An analogous situation is found for the $TiSc_2N@C_{80}^-$ anion and $Sc_3N@C_{80}^{2-}$ dianion.

TABLE 1. Relative Energies of $TiSc_2N@C_{80}$ Conformers in Neutral, Monocationic, and Monoanionic States and Isoelectronic Charge States of $Sc_3N@C_{80}$ Computed at the PBE/TZ2P and B3LYP/6-311G* Levels of Theory (kJ/mol)

|	1 (C_s)		2 (C_s)		3 (C_{3v})		4 (C_3)	
	PBE	B3LYP	PBE	B3LYP	PBE	B3LYP	PBE	B3LYP
$TiSc_2N@C_{80}^+$	1.9	0.8	0.0	0.0	1.6	3.8	0.5	4.1
$Sc_3N@C_{80}$	4.8	0.7			8.9	5.5	0.0	0.0
$TiSc_2N@C_{80}$	0.8	0.3	0.0	0.0	0.3	1.1	13.3	21.2
$Sc_3N@C_{80}^-$	3.8	2.3			0.0	0.0	13.4	27.1
$TiSc_2N@C_{80}^-$	1.0	0.0	1.6	6.8	0.0	4.8	29.9	
$Sc_3N@C_{80}^{2-}$	3.3	6.2			0.0	0.0	21.7	34.3

C_3-based structures are further destabilized (at the B3LYP level we did not find a minimum for **4**; optimization of the structure resulted in the conformer **1**), while **1**, **2**, and **3** have close energies (PBE favors the conformer **3**, which agrees well with the lowest energy found for the C_{3v} conformer of $Sc_3N@C_{80}^{2-}$, while B3LYP predicts that the conformer **1** is the most stable structure). For the $TiSc_2N@C_{80}^+$ cation, all four conformers are isoenergetic within 2 kJ/mol. Thus, in the positively charged state, the conformer **4** is not as destabilizing as for the neutral and anionic states, which also agrees with the fact that for the noncharged $Sc_3N@C_{80}$ the C_3 conformer has the lowest energy. In summary, these calculations have shown that there are apparent parallels between the relative energies of $Sc_3N@C_{80}$ and $TiSc_2N@C_{80}$ conformers in corresponding charge states.

In all conformers a substitution of Sc by Ti results in significant changes of the cluster bond lengths. Ti–N and Ti–C bonds (1.875 and 2.174 Å, respectively, in the conformer **3** at the B3LYP/6-311G* level of theory) are shorter than the corresponding Sc analogues (1.995 and 2.287 Å in C_{3v}-$Sc_3N@C_{80}^-$). As a result, the Sc–N bonds in the $TiSc_2N$ cluster (2.096 Å in the conformer **3**) are elongated in comparison to the Sc_3N values, and the nitrogen atom is displaced from the center of the molecule toward the titanium atom. Similar changes in the cluster parameters are known for the $Ln_xSc_{3-x}N@C_{80}$ mixed nitride clusterfullerenes (where Ln denotes Y and lanthanides), however, in all $Ln_xSc_{3-x}N@C_{80}$ molecules known so far, these were the Sc–N bonds that were shortened in comparison to Sc–N bonds of $Sc_3N@C_{80}$, while the Ln–N bonds were elongated in comparison to $Ln_3N@C_{80}$.[42,43,45–47,61]

Cluster Dynamics. The relative energies of different conformers of $TiSc_2N@C_{80}$ fall in the very small range, which points to the possible rotation of the $TiSc_2N$ cluster, just like it happens with the Sc_3N cluster in $Sc_3N@C_{80}$. However, the small difference in the energies of the conformers is not a sufficient proof of the cluster rotation by itself, since the barrier to the rotation can be large at the same time. To achieve the deeper understanding of the dynamical situation of the $TiSc_2N$ cluster, we have performed Born–Oppenheimer molecular dynamics (BOMD) simulations of $TiSc_2N@C_{80}$ at the PBE/DZ(P) level of theory (that is, the basis set of DZ quality was used for the carbon atoms of the fullerene cage, while the nitrogen and metal atoms were treated using DZP-quality basis set). Analogous calculations were also performed for $Sc_3N@C_{80}$ and $Sc_3N@C_{80}^-$.

In line with all previous experimental and theoretical findings,[15,37,56–60] BOMD simulations show that Sc_3N exhibits almost free rotation in $Sc_3N@C_{80}$ (not shown). Similar free rotation was also found in the $Sc_3N@C_{80}^-$ anion, in spite of the fact that the barriers to rotation of the cluster are predicted to be higher in the anion than in the neutral state.[12] Figure 4 shows the trajectory of $Sc_3N@C_{80}^-$ followed for 16 ps in the microcanonical en-
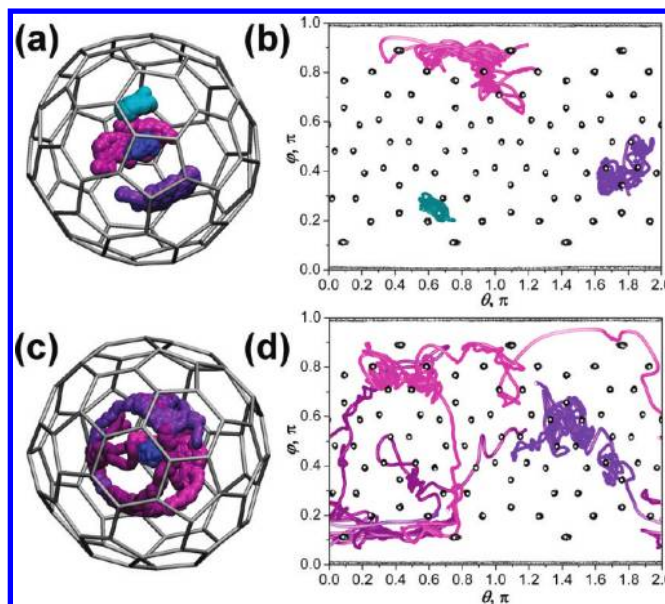
Figure 4. BOMD trajectories of $TiSc_2N@C_{80}$ (a, b) and $Sc_3N@C_{80}^-$ (c, d): Ti atom is cyan, Sc atoms are in different shades of magenta and violet, nitrogen atom is blue, and carbon atoms are gray. In (a) and (c) molecular presentations of trajectories are given (displacement of the carbon atoms are not shown); in (b) and (d) the trajectories are shown in polar coordinates (only angular part) emphasizing rotational component of the displacements.

semble after equilibration for 0.6 ps at 300 K. During this relatively short time, position of the Sc_3N cluster rearranged completely, the Sc atoms exhibiting long irregular trajectories covering substantial part of the inner surface of the carbon cage. Obviously, on the experimentally relevant time scale (for instance, nanoseconds for X-band ESR measurements) the cluster motion can be described as free rotation. Substantially different dynamical behavior in the same conditions is found for the $TiSc_2N$ cluster in $TiSc_2N@C_{80}$ (Figure 4a). During the whole 18 ps period, for which the trajectory was followed, the Ti atom remained almost fixed exhibiting only oscillations close to one pentagon/hexagon (pent/hex) edge of the carbon cage. The amplitudes of these oscillations are much higher than those for the carbon atoms, but are much smaller than those found for the Sc atoms in $Sc_3N@C_{80}$. As to the Sc atoms of the $TiSc_2N@C_{80}$, their dynamic behavior is close to that of $Sc_3N@C_{80}$ with large amplitude motions covering large parts of the cage. However, the motions of the Sc atoms in $TiSc_2N@C_{80}$ are somewhat frustrated compared to those in $Sc_3N@C_{80}$. Thus, the $TiSc_2N$ cluster dynamics can be described as restricted rotation around the Ti–N axis, which in due turn performs oscillations around the centre of one of the pent/hex edges of the carbon cage.

This result encouraged us to get more detailed information on the cluster rotation around the Ti–N axis, and we have analyzed a profile of potential energy surface (PES) along the cluster rotation at the PBE/TZ2P level of theory. In these calculations, six other conformers of $TiSc_2N@C_{80}$ were found as well as a set of transi-
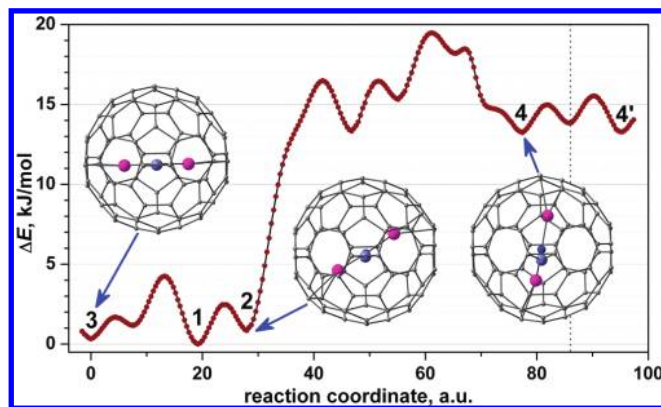
Figure 5. PBE/TZ2P energy profile along the rotation of the TiSc$_2$N cluster in TiSc$_2$N@C$_{80}$ around the Ti−N bond. Each point of the curve corresponds to one step in the intrinsic reaction coordinate calculations. Conformers **1**−**4** are denoted on the profile (**4′** is the symmetry equivalent of **4** with respect to the mirror plane of the carbon cage). Molecular structures of the conformers **2**, **3**, and **4** are also projected along the Ti−N bonds to emphasize rotation of the cluster.

tion states connecting the conformers (see Supporting Information for more details). Intrinsic reaction coordinate (IRC) calculations were then performed to reconstruct the energy profile. Figure 5 shows a representative fragment of the energy profile corresponding to the rotation of the cluster by 90°. It can be seen that rotation of the cluster can be described as a stepwise jumping between nine different conformers. Each step can be described as a rearrangement of usually one Sc atom from one pent/hex edge to another one, either in the same pentagon or in the neighboring pentagon (in the latter case transition state corresponds to Sc atom facing the center of the hexagon). This finding agrees with the results of BOMD simulations from this work as well as from ref 59 describing BOMD simulations for Sc$_3$N@C$_{80}$. It should be mentioned that the four conformers discussed in the previous section can be also obtained from each other by rotation of the cluster around Ti−N bond. If the rotation angle in conformer **3** is taken as a reference (0°), then the angles in other conformers are 27° in **1**, 33° in **2**, and 80° in **4** (Figure 5). Importantly, two regimes can be distinguished in the cluster rotation. The conformers **1**−**3**, as well as one newly found conformer, all have their energies below 2 kJ/mol and the barriers to the interconversion below 5 kJ/mol (Figure 5). These structures are, hence, easily accessible at room temperature, which agrees well with the results of our BOMD simulations. Further rotation requires a much higher barrier (16.5 kJ/mol). Once this barrier is overcome, five other conformers (including **4**) with relative energies in the range of 13−18 kJ/mol and barriers in the range of 15−20 kJ/mol can also be reached. Importantly, in our BOMD simulations, the cluster always remained in the first regime, and the higher energy structures have never been accessed in the 18 ps time scale.

The barriers to rearrangement of the Ti atom have also been studied. It was found that for the conform-

ers **1**−**3** rearrangement of the Ti atom between pent/hex edges of the same pentagon requires barriers of about 25−26 kJ/mol, while jumping to the pent/hex edge of another pentagon requires barriers of 11−13 kJ/mol.

In summary, both BOMD simulations and analysis of the energy profile show that the cluster dynamics can be described as rotation of the cluster around the Ti−N bond in a restricted range of rotation angles. Either rearrangement of the Ti atom or further rotation of the cluster require significantly higher barriers and such events have not been observed in our BOMD simulations. It is possible that at a longer time scale (which cannot be reached at this moment with our BOMD simulations) Ti atoms also perform ratchetlike jumping reorientations to other pent/hex edges, but in any case, it is obvious that the dwelling time of Ti atoms in one position is dramatically longer than that of Sc atoms. Hindered rotation of the cluster seems to be one of the reasons for the broadening of the ESR signal found for the TiSc$_2$N@C$_{80}$ at room temperature.

Molecular Orbital Analysis. Substantially different redox potentials observed for TiSc$_2$N@C$_{80}$ in comparison to Sc$_3$N@C$_{80}$ as well as different electronic absorption spectra[50] and dynamical properties indicate that replacement of one Sc atom by Ti results in strong changes in the electronic properties of the cluster-fullerene. Of course, these changes are in part explained by the surplus electron contributed by the Ti atom, but the difference in dynamic properties of the cluster between TiSc$_2$N@C$_{80}$ and Sc$_3$N@C$_{80}^-$ shows that the additional electron is not the only reason for the outlined differences. In this section we will analyze the difference in the electronic structure of TiSc$_2$N@C$_{80}$ and Sc$_3$N@C$_{80}$ in detail with the help of DFT calculations.

Figure 6 shows Kohn−Sham MO levels in TiSc$_2$N@C$_{80}^+$, TiSc$_2$N@C$_{80}$, Sc$_3$N@C$_{80}$, and Sc$_3$N@C$_{80}^-$. For the sake of clarity, in this analysis we used the C_{3v} conformer for Sc$_3$N@C$_{80}$ and the conformer **3** for TiSc$_2$N@C$_{80}$. When MO levels are uniformly shifted to adjust the difference in the MO levels in different charge states (in the cation MOs are stabilized, while in the anion they are destabilized), close similarities in the pairs TiSc$_2$N@C$_{80}^+$/Sc$_3$N@C$_{80}$ and TiSc$_2$N@C$_{80}$/Sc$_3$N@C$_{80}^-$ can be clearly seen in Figure 5. In both the TiSc$_2$N@C$_{80}^+$ and Sc$_3$N@C$_{80}$, the LUMO level is somewhat separated from the other unoccupied orbitals and, as can be seen in Figure 7, the LUMO is localized on the metal atoms of the cluster. However, in TiSc$_2$N@C$_{80}^+$, the contribution of Ti to LUMO is significantly larger than that of Sc atoms (Figure 7), and the orbital is stabilized by 0.378 eV compared to that in Sc$_3$N@C$_{80}$ (at the B3LYP/6-311G* level, the HOMO−LUMO gaps are 1.695 and 2.074 eV, respectively). When the LUMO is occupied by one electron, the single-occupied MO (SOMO) is stabilized with respect to the highest 2-fold occupied orbital, the gaps being 0.952 and 1.380 eV in TiSc$_2$N@C$_{80}$ or Sc$_3$N@C$_{80}^-$,
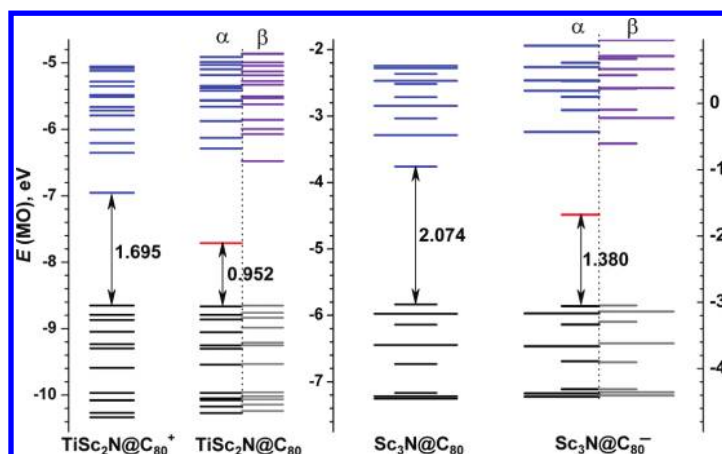
Figure 6. Kohn–Sham (B3LYP/6-311G*) MO levels of $TiSc_2N@C_{80}^+$, $TiSc_2N@C_{80}$, $Sc_3N@C_{80}$, and $Sc_3N@C_{80}^-$. Occupied levels are black (α) and gray (β), unoccupied levels are blue (α) and violet (β), and SOMO levels are red. For radicals, both α and β levels are shown. For the sake of comparison, the energy levels of $TiSc_2N@C_{80}^+$ and $Sc_3N@C_{80}^-$ are shifted to match the energies of the neutral $TiSc_2N@C_{80}$ and $Sc_3N@C_{80}$, which are shown in the same scale.

respectively. Here it can be seen again that the gap in $TiSc_2N@C_{80}$ is 0.427 eV smaller than in $Sc_3N@C_{80}^-$. At the same time, the energies of the highest 2-fold occupied orbitals in $TiSc_2N@C_{80}$ and $Sc_3N@C_{80}$ are virtually identical (−5.864 and −5.834 eV, respectively), and, as can be seen in Figure 7, these are essentially the cage orbitals, without significant metal contribution, and hence, they are virtually identical in both molecules.

The effect of the Ti atom, which stabilizes the LUMO by about 0.4 eV with respect to the analogues orbitals in $Sc_3N@C_{80}$, can be understood in the spirit of the Z+1 method, that is, considering that replacement of Sc by Ti is like an appearance of the core hole. The interaction of the hole with the valence electrons stabilizes to a larger extent those orbitals that are localized on the metal atom. This kind of interaction is also the reason of the preferable localization of the SOMO in $TiSc_2N@C_{80}$ on the Ti atom. The LUMO+1 in $Sc_3N@C_{80}$ (the next orbital after LUMO with the energy of 2.547 eV above HOMO) is 2-fold degenerate and also has significant metal contribution (Figure 7). In $TiSc_2N@C_{80}^+$ this orbital is split into two components (2.297 and 2.444 eV above HOMO). Thus, LUMO+1 components are also stabilized by replacement of Sc by Ti. Surprisingly, here the lower-energy component has a smaller Ti contribution.

Energetics of the Charged States. MO analysis clearly shows that the major difference in the redox properties of $TiSc_2N@C_{80}$ and $Sc_3N@C_{80}$ can be related to the presence of the electron on SOMO orbital in $TiSc_2N@C_{80}$, which is still vacant in the neutral $Sc_3N@C_{80}$ molecule. It can thus be expected that $TiSc_2N@C_{80}$ should be easier both to oxidize and to reduce than $Sc_3N@C_{80}$, because the energy of SOMO in $TiSc_2N@C_{80}$ is between the energies of HOMO and LUMO in $Sc_3N@C_{80}$. This reasoning perfectly agrees with the results of electrochemical measurements discussed above (Figure 1). DFT calculations also show that the adiabatic ionization potential (IP) of $TiSc_2N@C_{80}$, 5.77 eV (B3LYP/6-

311G*) or 6.18 eV (PBE/TZ2P), is noticeably smaller than that of $Sc_3N@C_{80}$ (6.88 or 6.62 eV at the B3LYP/6-311G* or PBE/TZ2P levels, respectively). In these calculations, the singlet state of $TiSc_2N@C_{80}$ was used, in which the electron is removed from the SOMO of $TiSc_2N@C_{80}$. If, however, a triplet state of the $TiSc_2N@C_{80}$ is considered, in which the electron is removed from the cage orbital just like in the oxidation of $Sc_3N@C_{80}$, then the corresponding IPs are computed to be 6.99 eV (B3LYP) or 6.73 (PBE), the values that are only 0.10 eV larger than those of $Sc_3N@C_{80}$.

The adiabatic electron affinities (EA) predicted for $TiSc_2N@C_{80}$, 2.77 eV (B3LYP) or 2.86 eV (PBE), are somewhat larger than those predicted for $Sc_3N@C_{80}$, 2.60 eV (B3LYP) or 2.83 eV (PBE; the experimental EA value for $Sc_3N@C_{80}$ is 2.81 eV[62]); however, the differences are not as strong as for the IP values. This is explained by the fact that, upon reduction, the electron goes to the orbital of the same type in both molecules, although in $TiSc_2N@C_{80}$ this MO is already occupied by one electron. Taking into account the deficiencies of DFT and the absence of solvation corrections, the differences in EA and IP values for $Sc_3N@C_{80}$ and $TiSc_2N@C_{80}$ agree rea-

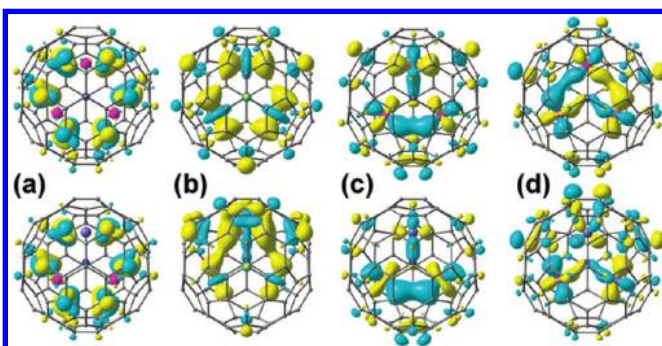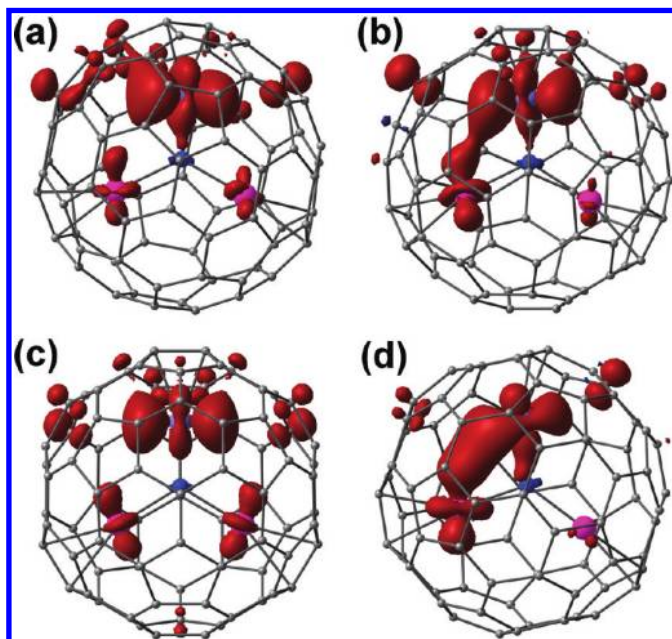Figure 7. Isosurfaces of the frontier orbitals of C_{3v}-$Sc_3N@C_{80}$ (top row) and **3**-$TiSc_2N@C_{80}^+$ (bottom row): (a) HOMO, (b) LUMO, (c) LUMO+1, (d) LUMO+2. In $Sc_3N@C_{80}$, LUMO+1 and LUMO+2 are 2-fold degenerate. The shapes of the orbitals in $TiSc_2N@C_{80}^+$ and $TiSc_2N@C_{80}$ are indistinguishable.

Figure 8. Spin density distribution (B3LYP/6-311G* level) in the conformers of $TiSc_2N@C_{80}$: (a) **1**, (b) **2**, (c) **3**, (d) **4**. Sc and Ti are shown in magenta and cyan, respectively.

sonably with the results of electrochemical measurements.

There is a certain similarity between $CeLu_2N@C_{80}$ and $TiSc_2N@C_{80}$ in that both molecules are radicals with an unpaired electron localized to a large extent on the metal (Ce or Ti) atoms. Both compounds are easier to oxidize in comparison to their diamagnetic analogues ($Lu_3N@C_{80}$ and $Sc_3N@C_{80}$, respectively) because oxidation results in the removal of the metal-localized unpaired electron. For both radicals the oxidation to the virtual state in which the electron is removed from the highest 2-fold occupied orbital of the carbon cage requires nearly the same energy as the oxidation of the diamagnetic analogues $Lu_3N@C_{80}$ or $Sc_3N@C_{80}$. The difference between $CeLu_2N@C_{80}$ and $TiSc_2N@C_{80}$ is found in the reduction, which occurs *via* occupation of metal-based SOMO in $TiSc_2N@C_{80}$ and the cage-based orbital in $CeLu_2N@C_{80}$.[54]

Spin Density Distribution. MO analysis shows that an unpaired electron in $TiSc_2N@C_{80}$ is largely localized on the Ti atom; that is, the valence state of Ti can be formally described as Ti(III). The spatial localization of the unpaired electron can be even better analyzed by means of spin density distribution shown in Figure 8 for the four conformers of $TiSc_2N@C_{80}$. In line with MO shapes, spin density is mostly localized on the $TiSc_2N$ cluster and, in particular, on the Ti atom. At the B3LYP/6-311G* level, the net Mulliken spin populations for the whole cluster in **1**, **2**, and **3** are in the range of 0.70 and, from that, 0.50−0.60 is contributed by Ti, nitrogen has a small negative spin population (−0.03), while the spin population of Sc atoms varies from conformer to conformer but does not exceed 0.17. In the conformer **4**, the spin population of the cluster is increased to 0.96,

from that population for Ti atom is 0.70, and the population for one of the Sc atoms is as large as 0.33. At the GGA PBE/TZ2P level, the spin distribution is qualitatively the same, but GGA tends to give larger Mulliken spin populations of the cluster in general (close to 1.00) and for the Ti atom in particular (*ca.* 0.90). Note that Hirschfeld spin populations computed at the PBE/TZ2P level appear to be closer to the Mulliken populations computed at the B3LYP/6-311G*. While exact values can vary from method to method, the qualitative description is the same and agrees with MO analysis, showing the three-valent state of Ti atom with an unpaired d-electron.

Spin Dynamics. An important conclusion based on the analysis of the spin density distribution is that a reorientation of the cluster is accompanied by the spin flow between the metal atoms in the cluster and between the cluster and the cage. We have recently described similar flexibility of the spin distribution in the studies of the different conformers of the $Sc_3N@C_{80}^-$ anion radical.[12] To get a deeper insight into the dynamics of the spin flow we have analyzed the evolution of the spin populations in the BOMD trajectories described above. Figure 9 plots the spin populations of the Ti, Sc, and N atoms in $Sc_3N@C_{80}^-$ and $TiSc_2N@C_{80}$ as a function of time. The spin populations experience a significant variation with time in both studied radicals. In $Sc_3N@C_{80}^-$, the spin population of Sc atoms oscillates in the range of ±0.25 about the averaged value of 0.29, the nitrogen atom exhibits negligible variations of the population (the value averaged over the trajectory is −0.04), and the net spin population of the whole cluster mostly remains in the range of 0.83 ± 0.15 (with few dips down to 0.50−0.60). A different scenario of the spin dynamics is observed in $TiSc_2N@C_{80}$. At the PBE/DZ(P) level used for the BOMD simulations, the population for Ti atom averaged over the trajectory is 0.97, and the value varies in the range of about ±0.15 (the maximum deviations reaching 0.22). Sc atoms have much smaller average populations, 0.06, and the values deviate within the range of about ±0.05 (the maximum deviation is 0.12). The net spin population of the $TiSc_2N$ cluster lies within the range of 1.02 ± 0.10 (the maximum deviations, coinciding in time with the maximum deviations for Ti atom, are at the order of 0.16). It can be seen that in both molecules the deviations of the net spin populations of the cluster are considerably smaller than those of the individual metal atoms. This shows that both an intracluster and a cluster-cage spin exchange take place.

Taking the dynamical nature of the spin distribution in the clusterfullerenes into account does not change the main conclusion about the preferential localization of the spin density on the Ti atom in $TiSc_2N@C_{80}$. However, it can be seen already in the time domain that the spin population for Ti shows regular oscillations, and the periodicity can be even better

seen for the autocorrelation function (not shown). Fourier transformation of the autocorrelation function transforms the dependence into the frequency domain, thus, allowing the more detailed analysis of the spin flow channels. The spin-flow vibrational spectra obtained as a result of the Fourier transformation of the autocorrelation functions for spin populations of the Ti, Sc, and N atoms as well as the net spin population of the $TiSc_2N$ cluster are shown in Figure 10a (Fourier transformation of the dependences themselves yields qualitatively the same spectra but with somewhat higher level of noise).

To relate the peaks in the spin-flow vibrational spectra to the motions of the cluster we have performed Hessian computations of the conformers **1**−**4**. Although BOMD gives averaged information on all thermally accessible conformers, it is still possible to use the normal modes computed for specific conformers for such an analysis because vibration of a similar type in different conformers occurs in the narrow frequency range (usually a few cm^{-1}). Hence, the frequency of the peaks in the BOMD-derived spectra are very close to the vibrational frequencies of the individual conformers (however, they are usually not identical because the former correspond to the mean value for several structures).

The highest amplitude of the spin population variation for the Ti atom is observed at 87 cm^{-1}. Hessian computations show that this frequency corresponds to the libration of the $TiSc_2N$ cluster as a whole, with the largest displacement exhibited by the Ti atom (see Figure 10b). In fact, the displacement of the Ti atom observed in BOMD (Figure 4) is largely caused by this vibration. Because this mode has a high activity for both Ti and the whole cluster, this mode is considered to be the major channel for the spin flow between the cluster and the carbon cage. However, this mode is also one of the most active for Sc atoms, and hence, it is also a major channel for the intracluster spin exchange.

Amplitudes of the spin population variation for the Ti atom that are an order of magnitude lower than that for the 87 cm^{-1} mode are found for the vibrations at 262, 314, and 601 cm^{-1}. In the conformer **3**, the former corresponds to the two modes at 259 and 261 cm^{-1}, with a large contribution from the out-of-plane motion of the nitrogen atom (in other conformers, analogous modes are found at close frequencies). The peak at 314 cm^{-1} is due to the vibrational mode at 317 cm^{-1}, which is basically the cage vibration with some contribution of the Ti−N stretching. Finally, the peak at 601 cm^{-1} corresponds to the component of the antisymmetric metal−nitrogen stretching mode, with the predominant contribution of Ti−N stretching. This mode is characteristic for the metal-nitride clusterfullerenes and can be described as the in-plane motion of the nitrogen atom, with the metal atoms remaining intact. In $M_3N@C_{80}$ clusterfullerenes (with homogeneous metal
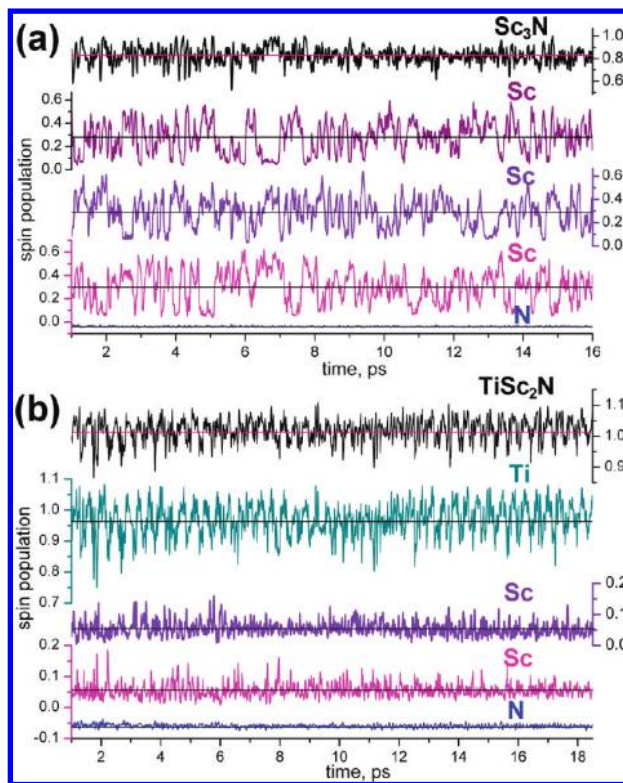
Figure 9. Spin populations for Sc, Ti, N atoms and Sc_3N (a) and $TiSc_2N$ (b) clusters as a function of time obtained in the Born−Oppenheimer molecular dynamics at the PBE/DZ(P) level. Dark horizontal lines show the average values over the trajectory.

clusters), the mode is 2-fold degenerate.[21,34,63] In the mixed cluster, the degeneracy is lifted, and the splitting of the two components can reach 200 cm^{-1}.[43,45−47,49] In particular, for $TiSc_2N@C_{80}$, our FTIR vibrational spectroscopy study revealed a splitting of about 100 cm^{-1}.[50] The component at 600 cm^{-1} corresponds to the motion of the nitrogen atom along the Ti−N bond, while the perpendicular motion of the nitrogen atom (parallel to the Sc⋯Sc vector) occurs at about 510 cm^{-1}. Note that the peaks at 261 and 314 cm^{-1} appear for both Ti and the whole cluster, while the peak at 601 cm^{-1} has no counterpart for the whole cluster (Figure 10b). Thus, the antisymmetric metal−nitrogen stretching mode, being the channel for the intracluster spin flow, does not cause the spin exchange between the cluster and the cage.

An analysis of the amplitudes of the spin population variation for the Sc atoms shows that there is no special exchange channel for these atoms (like the mode at 87 cm^{-1} for Ti). Instead, there are several modes with similar amplitudes. In addition to the aforementioned vibration at 87 cm^{-1}, large amplitudes are found for the modes at about 200 cm^{-1}, which correspond to the Ti−N−Sc and Sc−N−Sc deformations. Because the corresponding peaks are absent for both Ti atom and the whole cluster, these modes are channels of the spin exchange between the two Sc atoms. Considerable amplitudes of the spin population varia-
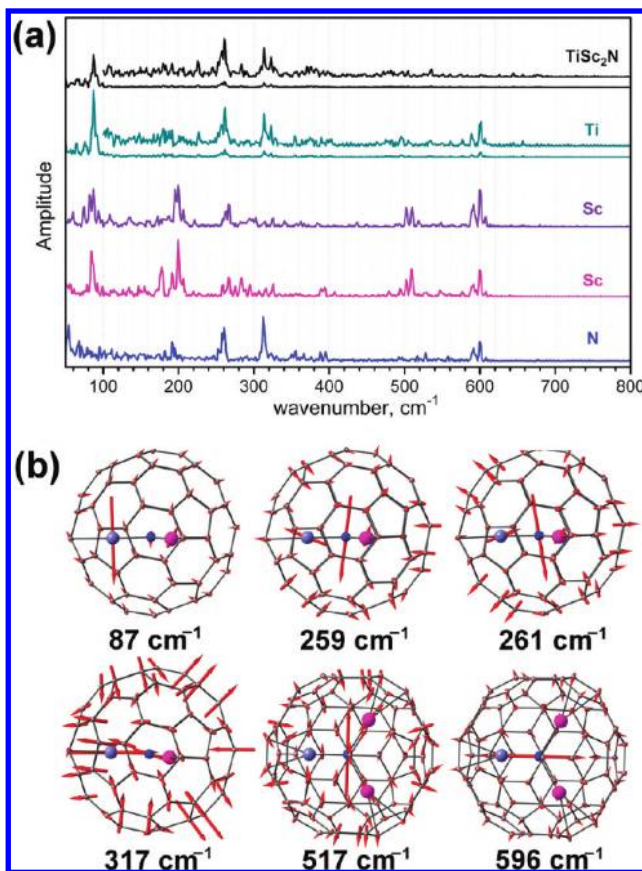
Figure 10. (a) Spin-flow vibrational spectra obtained as a result of Fourier transformation of the autocorrelation function of the time-dependent spin populations (for TiSc$_2$N and Ti, the insets show an enhanced higher frequency part); (b) vibrational displacement corresponding to the most prominent peaks in (a).

tion are also found at around 510 and 600 cm^{-1}, with the frequencies corresponding to the two components of the antisymmetric metal−nitrogen stretching mode, as discussed above. While for Ti atom only the higher-frequency vibration has a considerable amplitude, for Sc atoms, both components are active. The lower-frequency mode, which is basically the Sc−N antisymmetric stretching mode, is another channel for the spin exchange between the Sc atoms without participation of the rest of the molecule.

Based on the analysis of the spin-flow vibrational spectra outlined above, it can be concluded that the noticeable flow of the spin density between the cluster and the cage occurs only when the metal atoms are involved in the vibrations. The antisymmetric metal−nitrogen stretching, though producing noticeable amplitudes of the spin population variations for the metal atoms, is "silent" for the cluster as a whole. It is also worth noting that when the metal atoms remain in place, motions of the nitrogen atom can modulate the spin exchange between them. The fact that the spin flow between the cluster and the cage is selectively coupled to a single vibrational mode at 87 cm^{-1} is quite remarkable. It shows that TiSc$_2$N@C$_{80}$ might be a useful

material for spin transport in the conditions of selective excitation of this vibration by, for instance, an AFM tip.

Surprisingly, the spin-flow vibrational spectroscopy, that is, coupling BOMD with observation of the spin density distribution of molecular materials, although essentially simple, has to our knowledge not been described in the literature. Our work shows that this method can be very useful in the understanding of the dynamics of spin density distribution and can provide valuable information on the coupling between the spin states and the internal dynamics of the molecules.

Chemical Bonding and the Role of Ti(III). Based on the Ti(III) state of the titanium atom with highly localized d-electron it might be suggested that parameters of the Ti-cage bonding in TiSc$_2$N@C$_{80}$ are similar to those of the Sc-cage bonding. At the same time, a removal of one electron (which is therefore essentially removed from Ti) transforms titanium into the formal Ti(IV) state, while addition of one electron results in Ti(II). Because TiSc$_2$N@C$_{80}^+$ is isoelectronic to Sc$_3$N@C$_{80}$, it might be also expected that the Ti-cage bonding in the cation is similar to the Sc-cage bonding in Sc$_3$N@C$_{80}$. On the other hand, studies of the bonding in Ti$_2$C$_2$@C$_{78}$ with the tetravalent Ti(IV) revealed a considerably enhanced degree of covalency of the metal-cage bonding when compared to Sc-based endohedral fullerenes,[41,64] and it is an open question whether a similar phenomenon takes place in TiSc$_2$N@C$_{80}$.

To address these questions in this work, we have analyzed the bonding in TiSc$_2$N@C$_{80}$ in different charge states using quantum theory of atoms in molecules (QTAIM),[65,66] which was employed by us recently to study the bonding in different classes of endohedral metallofullerenes.[41] From the many parameters provided by QTAIM, we will preferably use atomic charges, q(M), and delocalization indices, δ(A, B), which quantify the number of the electron pairs shared between A and B. In other words, δ(A, B) can be described as the A−B bond order. Note that A or B are not necessarily single atoms; in particular, in the following analysis we will use δ(M, cage), the number of electron pairs shared between the metal atom and the carbon cage (that is, the "metal-cage bond order"), obtained as a sum of all individual δ(M, C$_{cage}$) values. Besides, the sum of all δ(M, B) indices, where B denotes all atoms in the molecule except for M itself, can be understood as the "valence" of M and will be denoted hereafter as ΔM. Table 2 lists some of the results of the QTAIM analysis performed for the conformer **3** and its cation and anion (note that for the charged states the coordinates optimized for the neutral form were used in the calculations of the electronic density). For comparison, analogue calculations were also performed for 0, −1, and −2 charge states of the C_{3v} conformer of Sc$_3$N@C$_{80}$; for the sake for comparison, coordinates optimized for the monoanion were used in all calculations.

TABLE 2. Selected Charges and Delocalization Indices Obtained by the QTAIM Analysis of TiSc$_2$N@C$_{80}^{+,0,-}$, Sc$_3$N@C$_{80}^{0,-,2-}$, Ti(Cp)$_2$CH$_3^{+,0,-}$ and Ti(Cp)$_2$(CH$_3$)$_2$^{a}

molecule	M	q(M)	q(N/C)^b	q(M$_3$N)	δ(M, N/C)^c	δ(M, Sc)	δ$_{max}$(M, C$_{cage}$)^d	δ(M, cage)^e	ΔM
TiSc$_2$N@C$_{80}^+$	Ti	2.318	−1.879	3.942	0.942	0.039	0.242	2.194	3.214
	Sc	1.752			0.573	0.022	0.230	1.940	2.575
TiSc$_2$N@C$_{80}$	Ti	2.190	−1.905	3.770	0.938	0.068	0.236	2.158	3.232
	Sc	1.743			0.605	0.033	0.220	1.871	2.576
TiSc$_2$N@C$_{80}^-$	Ti	2.164	−1.922	3.664	0.937	0.095	0.235	2.268	3.395
	Sc	1.711			0.614	0.054	0.212	1.885	2.648
Sc$_3$N@C$_{80}$	Sc	1.764	−1.772	3.519	0.744	0.042	0.199	1.748	2.576
Sc$_3$N@C$_{80}^{-f}$	Sc	1.714	−1.791	3.351	0.754	0.079	0.188	1.731	2.644
Sc$_3$N@C$_{80}^{2-}$	Sc	1.691	−1.803	3.272	0.756	0.084	0.184	1.772	2.695
Ti$_2$C$_2$@C$_{78}^f$	Ti	1.670	−0.587		0.805		0.349	3.291	4.109
Ti(Cp)$_2$CH$_3^+$	Ti	2.329	−0.596		0.709		0.243	2.367	3.076
Ti(Cp)$_2$CH$_3$	Ti	2.031	−0.548		0.651		0.285	2.475	3.126
Ti(Cp)$_2$CH$_3^-$	Ti	1.918	−0.519		0.617		0.351	2.815	3.432
Ti(Cp)$_2$(CH$_3$)$_2$	Ti	2.322	−0.502		0.627		0.201	1.869	3.123
Ti@C$_{28}$	Ti	2.280					0.270	3.368	3.368

^{a}B3LYP/6-311G* calculations. ^{b}Charge of the carbon atom in the carbide unit in Ti$_2$C$_2$@C$_{78}$ or in the CH$_3$ group in Ti(Cp)$_2$CH$_3$ and Ti(Cp)$_2$(CH$_3$)$_2$. ^{c}δ(Ti, C$_2$) value for Ti$_2$C$_2$@C$_{78}$ and δ(Ti, CH$_3$) for Ti(Cp)$_2$CH$_3$ and Ti(Cp)$_2$(CH$_3$)$_2$. ^{d}δ$_{max}$(Ti, C$_{cp}$) for Ti(Cp)$_2$CH$_3$ and Ti(Cp)$_2$(CH$_3$)$_2$; ^{e}δ(Ti, (Cp)$_2$) for Ti(Cp)$_2$CH$_3$ and Ti(Cp)$_2$(CH$_3$)$_2$; ^{f}From ref 41.

A comparison of the QTAIM parameters for Ti atom in TiSc$_2$N@C$_{80}$ to those of Sc in Sc$_3$N@C$_{80}$ and TiSc$_2$N@C$_{80}$ shows a considerable difference in the bonding situation. First, atomic charges of Ti are about 0.5 $\bar{e}$ more positive than those of Sc, while the charge of the nitrogen atom in Sc$_2$TiN@C$_{80}$ is about 0.1 $\bar{e}$ more negative than in Sc$_3$N@C$_{80}$. Because the charges of Sc atoms are similar in two types of clusters, the net charges of the nitride cluster are about 0.4 $\bar{e}$ more positive for Sc$_2$TiN in the corresponding isoelectronic charge states. At the same time, the Ti−N bond exhibits a higher degree of covalency as revealed by the δ(Ti, N) values, which are about 0.2 and 0.3 higher than δ(Sc, N) values in Sc$_3$N and TiSc$_2$N clusters, respectively. In fact, the δ(M, N) indices show a reasonable correlation with the metal−nitrogen bond lengths: the longer the bond, the smaller the delocalization index.

The situation in the metal-cage bonding is also different in TiSc$_2$N@C$_{80}$ and Sc$_3$N@C$_{80}$. In particular, both δ(Ti, cage) and δ(Sc, cage) indices are about 0.45 and 0.15, respectively, larger in TiSc$_2$N@C$_{80}$ than the δ(Sc, cage) indices in Sc$_3$N@C$_{80}$. In due turn, Ti exhibits a considerably stronger covalent bonding to the carbon cage than the Sc atoms, which is in line with the lower mobility of Ti atoms revealed by the BOMD study. Finally, the ΔM values for Ti are also about 0.6 larger than the corresponding values for Sc, showing the higher valency of Ti. At the same time, in spite of a considerable difference in Sc−N and Sc-cage bonding in TiSc$_2$N@C$_{80}$ and Sc$_3$N@C$_{80}$, ΔM values for Sc atoms are very similar in two clusterfullerenes, irrespective of the charge state. Thus, the decreased covalency of the Sc−N bonds in TiSc$_2$N@C$_{80}$ is compensated by the increased covalency of the Sc-cage interactions. Note that just like already mentioned for Sc, the ΔM values for Ti are weakly changing with the charge of TiSc$_2$N@C$_{80}$ (from 3.2 in the monocation to 3.4 in the monoanion). That is, based

on the charges, delocalization indices, and ΔM, it is concluded that the actual valence state is essentially the same for the Ti atom in different charge states of TiSc$_2$N@C$_{80}$, while the formal valence of Ti is changing from Ti(II) in the anion to Ti(IV) in the cation. Comparison to the state of Ti in Ti$_2$C$_2$@C$_{78}$ shows that in the latter the charge of the Ti atom is much smaller (q = 1.67), the Ti-cage bonding is considerably stronger (δ(Ti, cage) = 3.29) and, hence, the ΔM value (4.11) is considerably larger than in TiSc$_2$N@C$_{80}$. Bonding situation is thus considerably different for Ti atom in carbide and nitride clusterfullerenes.

The shape of the SOMO in TiSc$_2$N@C$_{80}$ and Sc$_3$N@C$_{80}$ suggests a weak metal−metal bonding character, which can be enhanced by a further occupation of this orbital. Based on the SOMO shape in C$_{3v}$-Sc$_3$N@C$_{80}^-$, Valencia *et al.* have also pointed out that enhanced Sc⋯Sc bonding interactions might be the reason for the increased stability of the C$_{3v}$ conformer (in other conformers these interactions are less pronounced).[60] In this respect, we have analyzed the Ti−Sc and Sc−Sc delocalization indices in different charge states of **3**-TiSc$_2$N@C$_{80}$ and C$_{3v}$-Sc$_3$N@C$_{80}$. As shown in Table 2, the population of the cluster-based orbital results in an increase of the δ(Ti, Sc) and δ(Sc, Sc) values. For instance, the δ(Ti, Sc) index is increased from 0.039 in TiSc$_2$N@C$_{80}^+$ to 0.095 in TiSc$_2$N@C$_{80}^-$, while the δ(Sc, Sc) index is growing from 0.042 in Sc$_3$N@C$_{80}$ to 0.084 in Sc$_3$N@C$_{80}^{2-}$. However, these values are still rather small, and it is difficult to correlate them with the stability of the conformers. Note that, among the four conformers of TiSc$_2$N@C$_{80}$ studied in this work, the largest δ(Ti, Sc) index, 0.19, is found in the relatively unstable conformer **4** (see Figure 8 for the spin density distribution).

Spin-Charge Separation. The changes of the valence states of Sc and Ti atoms with the charge of the cluster-
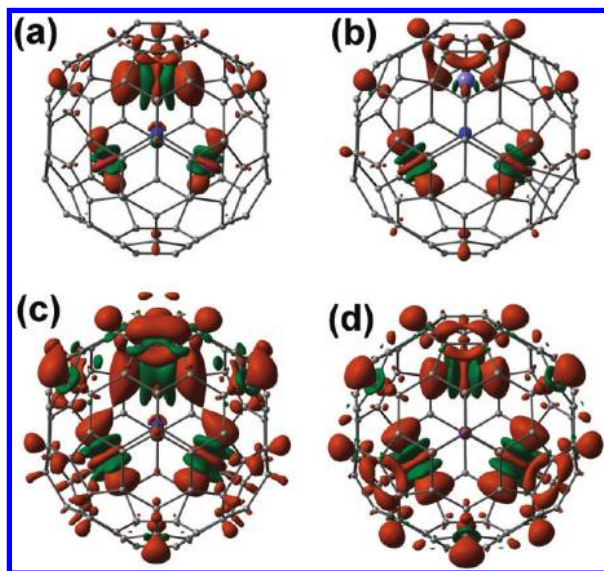
Figure 11. Isosurfaces of the difference densities (B3LYP/6-311G* level): (a) $[\rho(TiSc_2N@C_{80}) - \rho(TiSc_2N@C_{80}^+)]$; (b) $[\rho(TiSc_2N@C_{80}^-) - \rho(TiSc_2N@C_{80})]$; (c) $[\rho(TiSc_2N@C_{80}^-) - \rho(TiSc_2N@C_{80}^+)]$; (d) $[\rho(Sc_3N@C_{80}^{2-}) - \rho(Sc_3N@C_{80})]$.

fullerenes deserve a special attention. Importantly, a removal of one electron, which, according to the SOMO shape and spin population, should result in about a $+0.5\ \bar{e}$ increase of the q(Ti) value in $TiSc_2N@C_{80}$, actually gives a much smaller increase of $+0.13\ \bar{e}$. Likewise, an addition of one electron to $TiSc_2N@C_{80}$ reduces the charge by only $-0.03\ \bar{e}$ in spite of the total localization of the LUMO on the cluster and in particular on the Ti atom. Thus, on passing from $TiSc_2N@C_{80}^+$ to $TiSc_2N@C_{80}^-$ via population of the cluster-based MO by two electrons, the charge of the cluster is changed by only $-0.28\ \bar{e}$ and the charge of the Ti atom by only $-0.15\ \bar{e}$. These values contradict the changes of the spin population (from 0.5 to 0 in the cation and anion) and point to the spatial charge-spin separation (that is, while the spin is changed on the cluster, the charge changes occur on the carbon cage). Earlier we have found a similar phenomenon for some other endohedral fullerenes with metal-localized LUMO (SOMO).[12] In such molecules, a change of the charge state resulted in the localization of the spin density on the metal atoms but was not accompanied by the corresponding changes in the atomic charges. To clarify this point, we have plotted differences in the electronic densities between the different charge states of $TiSc_2N@C_{80}$ (Figure 11). The $[\rho(TiSc_2N@C_{80}) - \rho(TiSc_2N@C_{80}^+)]$, $[\rho(TiSc_2N@C_{80}^-) - \rho(TiSc_2N@C_{80})]$, and $[\rho(TiSc_2N@C_{80}^-) - \rho(TiSc_2N@C_{80}^+)]$ differences (Figure 11a–c) reveal large changes in the local electron density distribution of the metal atoms (and in particular Ti) caused by the change of the total charge, but these changes are rather *reorganizations* than *depletions*, because in all cases the change of the electronic density is compensated by the appearance of the lobes with the opposite sign. As a result, the total change of the metal charges is

rather small, while the small changes of the electronic densities in the carbon atoms of the cage are not compensated by the lobes with the opposite sign and therefore sum up into the relatively large net values. The same effect can be seen for $Sc_3N@C_{80}$ on passing from the neutral to the dianionic state (Figure 11d); the only difference is that the local changes of the density are more enhanced for the Ti atom in $TiSc_2N@C_{80}$ and are uniformly distributed over all three Sc atoms in $Sc_3N@C_{80}$.

To clarify whether this situation is specific to the bonding in endohedral metallofullerenes or has a more general nature, the nonfullerene Ti compounds with carbocyclic π-ligands were considered and computations were performed for $Ti(Cp)_2CH_3$ and $Ti(Cp)_2(CH_3)_2$ (Cp = cyclopentadiene). The valence state of Ti in $Ti(Cp)_2CH_3$ mimics the situation in $TiSc_2N@C_{80}$ in that the two electrons are formally transferred to the Cp rings, which is equivalent to the electron transfer to the carbon cage in $TiSc_2N@C_{80}$, while the polar covalent Ti−CH₃ bond is similar to the Ti−N bond in $TiSc_2N@C_{80}$. Thus, Ti is in the formal Ti(III) state and has an unpaired d-electron (the spin population is 0.97, so the electron is more strongly localized on the Ti atom than in $TiSc_2N@C_{80}$ and the SOMO of $Ti(Cp)_2CH_3$ is respectively a pure 3d-orbital of Ti). Likewise, addition/removal of one electron to/from the molecule should result in the change of the charge states of Ti by almost 1 $\bar{e}$. Yet, even in this system the actual changes of the valence state of Ti are comparably small. On passing from the cation to the anion by populating the 3d-orbital of Ti by two electrons, the charge of the Ti atom is reduced by only 0.41 $\bar{e}$. The ΔM value is also changed by 0.35. Counterintuitively, population of the 3d-orbital of Ti, which formally yields the Ti in the lower valence state, increases its ΔM value. Thus, we can conclude that the spatial spin-charge separation is not specific to metallofullerenes but probably a general property of transition metals coordinated to the carbocyclic ligands. This phenomenon will be studied in more detail in future work.

To conclude this section, we have also studied $Ti(Cp)_2(CH_3)_2$, in which Ti is in the genuine Ti(IV) state and might be expected to be closer to $Ti_2C_2@C_{78}$ in its bonding situation. However, the charge and ΔM value of Ti in $Ti(Cp)_2(CH_3)_2$ are quite close to those in $TiSc_2N@C_{80}$ and $Ti(Cp)_2CH_3$. Finally, the computation was also performed for C_{3v}-$Ti@C_{28}$,[14] in which Ti formally donates four electrons to the T_d-C_{28} carbon cage. Here again we find the charge and ΔM value of the Ti atom to be not much different from those in $TiSc_2N@C_{80}$ and $Ti(Cp)_2CH_3$. Thus, it can be concluded that QTAIM charges of about 2.0−2.3 and ΔM values of 3.1−3.4 are typical for Ti coordinated to the carbocyclic ligands, and these values are almost independent of the formal valence state of Ti. The valence state of Ti in $Ti_2C_2@C_{78}$ with q(Ti) of +1.67 and ΔM of 4.1 is an exception rather

than the rule. This conclusion agrees well with the results of Hino *et al.*[64] and explains the fact that the determination of the valence state of Ti in $Ti_2C_2@C_{78}$ by EELS met some difficulties.[7]

CONCLUSIONS

In this work we have performed a detailed study of the electronic structure and dynamics of the mixed-metal nitride clusterfullerene $TiSc_2N@C_{80}$. In particular, the role of the Ti atom in $TiSc_2N@C_{80}$ was analyzed as compared to $Sc_3N@C_{80}$. It was found that substitution of Sc by Ti results in the reversible redox behavior of the new NCF, making $TiSc_2N@C_{80}$ different from all $M_3N@C_{80}$ NCFs known to date. $TiSc_2N@C_{80}$ is paramagnetic, but its room temperature ESR spectrum is strongly broadened, and only lowering the temperature results in an ESR signal with a g-factor of 1.9454. The significant shift of the g-factor from the free-electron value as well as the significant g-tensor anisotropy (*ca.* 0.08) point to the localization of the spin-density on the Ti atom, a conclusion also being confirmed by DFT computations.

The structure of $TiSc_2N@C_{80}$ in terms of the cluster orientation inside the carbon cage resembles that of the isoelectronic $Sc_3N@C_{80}^-$ and is different from $Sc_3N@C_{80}$. However, Born−Oppenheimer molecular dynamics simulations revealed that the cluster dynamics of $TiSc_2N$ is substantially different from that of Sc_3N in $Sc_3N@C_{80}$, irrespective of the charge of the latter. While Sc_3N exhibits free rotation inside the cage, the Ti atom appears to be fixed in one position (although with rather higher amplitudes of oscillations), and hence, the cluster exhibits only rotations around the Ti−N axis. The study of the atomic spin populations as a function of time revealed that both $Sc_3N@C_{80}^-$ and $TiSc_2N@C_{80}$ have flexible spin-density distribution with both intracluster and cluster-cage spin flow. Furthermore, the spin-flow vibrational spectra (obtained *via* Fourier transformation of the time-dependent spin populations) revealed that the spin flow in $TiSc_2N@C_{80}$ is not a random process, but is coupled to a specific cluster vibration. Thus, the approach referred to in this work as the "spin-flow vibrational spectroscopy" is shown to be a powerful tool in the study of the spin dynamics in molecules with flexible spin-density distribution. By this method, the major channels of the spin transfer in molecular systems are detectable and can be of high importance for the spin transport.

EXPERIMENTAL AND COMPUTATIONAL DETAILS

Synthesis and Isolation of $TiSc_2N@C_{80}$. The details of the synthetic procedure were described earlier.[50] In brief, a mixture of TiO_2 (99.99%) and Sc_2O_3 (99.99%) with graphite powder at certain Ti/Sc molar ratios ranging from 8:1 to 1:2 (typically 1:1, molar ratio of Sc/C is fixed at 1:15) was subjected to DC-arc discharging. The modified Krätschmer−Huffman DC-arc discharging was done in a 400 mbar He atmosphere under addition of N_2 (10 mbar). The as-produced soot was Soxhlet-extracted by CS_2 for 24 h, and the resulting brown-yellow solution was distilled to remove CS_2, redissolved in toluene (∼ 200 mL), and subsequently passed through a 0.2 μm Teflon filter (Sartorius AG, Germany) for further HPLC separation. The separation of $TiSc_2N@C_{80}$ was performed by a multistep HPLC, as described in a former work.[50] The purity of the isolated $TiSc_2N@C_{80}$ was further checked by LD-TOF MS analysis running in both positive and negative ion modes (Autoflex III, Bruker Daltonics Inc., Germany).

Experimental Measurements. For a cyclic voltammetry study, the $TiSc_2N@C_{80}$ sample dissolved in toluene was dried and transferred as a powder into a glovebox (oxygen and water content below 1 ppm), where it was immediately redissolved in 1,2-dichlorobenzene (*o*-DCB, anhydrous, 99%, Aldrich) with tetrabutylammonium tetrafluoroborate (TBABF$_4$, Fluka, dried under reduced pressure at 340 K for 24 h prior to use) used as the supporting electrolyte at concentrations of 0.1 mol L^{-1}. The cyclic voltammograms were obtained with a PAR 273 potentiostat (EG&G, U.S.A.) in a three-electrode system using platinum wires as working and counterelectrodes and a silver wire as pseudo-reference electrode under glovebox conditions. Ferrocene (Fc) was added as the internal standard at the end of voltammetric measurements and all potentials are given *versus* the Fc/Fc$^+$ couple.

ESR measurements in the temperature interval 100−300 K were performed using EMX X-band spectrometer (Bruker, Germany) and continuous-flow liquid-nitrogen cryostat, inserted in the ER 4102 ST resonator of the spectrometer. For the helium-temperature ESR measurements, a continuous-flow liquid-helium cryostat was used. This cryostat was inserted into the TE102 resonator of the EMX X-band ESR spectrometer (Bruker, Germany) and enabled the measurements down to about 4 K. The sample (toluene solution with concentration of *ca.* 0.5 mg/mL) was placed at the position of maximum microwave magnetic field inside the resonator. By adding a small ac modulation to the external magnetic field, lock-in detection was used, enabling high sensitivity of the detected ESR signal.

Computations. Optimization of the molecular structure of all species reported in this work was first performed using PBE functional[67] and TZ2P-quality basis set (full-electron {6,3,2}/(11s,6p,2d) for C and N atoms, and SBK-type effective core potential for Sc and Ti atoms with {5,5,4}/(9s,9p,8d) valence part) implemented in the PRIRODA package.[68,69] This basis set is abbreviated in the manuscript as TZ2P. The code-employed expansion of the electron density is an auxiliary basis set to accelerate evaluation of the Coulomb and exchange-correlation terms.[68] Optimization of the molecular structure at the B3LYP/6-311G* level was performed with the use of the Firefly package.[70] QTAIM (quantum theory of atoms in molecules) analysis of the electron densities was performed with the use of the AIMAll code (version 10.01.14, http://aim.tkgristmill.com).

Velocity Verlet algorithm with the time step 1.5 fs was used in Born−Oppenheimer molecular dynamics (BOMD) calculations. The energies and gradients were computed with PRIRODA using PBE functional, double-ζ quality {3,2}/(7s,4p) basis set for cage carbon atoms and DZP-quality basis sets for nitrogen, scandium, and titanium atoms (Sc, Ti: {6,5,3,1}/(19s,15p,11d,5f); N: {3,2,1}/(10s,7p,3d)). Molecules were first equilibrated at 300 K for 0.6 ps by rescaling velocities when the deviation of the instant temperature from 300 K exceeded 20 K. Then, the trajectory was followed without thermostat (i.e., in microcanonical ensemble).

REFERENCES AND NOTES

1. Akasaka, T.; Nagase, H. *Endofullerenes: A New Family of Carbon Clusters*; Kluwer: Dordrecht, 2002.
2. Shinohara, H. Endohedral Metallofullerenes. *Rep. Prog. Phys.* **2000**, *63*, 843–892.
3. Dunsch, L.; Yang, S. Metal Nitride Cluster Fullerenes: Their Current State and Future Prospects. *Small* **2007**, *3*, 1298–1320.
4. Chaur, M. N.; Melin, F.; Ortiz, A. L.; Echegoyen, L. Chemical, Electrochemical, and Structural Properties of Endohedral Metallofullerenes. *Angew. Chem., Int. Ed.* **2009**, *48*, 7514–7538.
5. Popov, A. A. Metal-Cage Bonding, Molecular Structures, and Vibrational Spectra of Endohedral Fullerenes: Bridging Experiment and Theory. *J. Comput. Theor. Nanosci.* **2009**, *6*, 292–317.
6. Greenwood, N. N.; Earnshaw, A. *Chemistry of the Elements*; Pergamon: Oxford, 1984.
7. Cao, B. P.; Hasegawa, M.; Okada, K.; Tomiyama, T.; Okazaki, T.; Suenaga, K.; Shinohara, H. EELS and ^{13}C NMR Characterization of Pure $Ti_2@C_{80}$ Metallofullerene. *J. Am. Chem. Soc.* **2001**, *123*, 9679–9680.
8. Hino, S. J.; Iwasaki, K.; Wanita, N.; Yoshimura, D.; Cao, B. P.; Okazaki, T.; Shinohara, H. Ultraviolet Photoelectron Spectroscopy of Two Titanium Metal Atoms Encapsulated Metallofullerenes, $Ti_2@C_{80}$ and $Ti_2@C_{84}$. *Fullerenes, Nanotubes, Carbon Nanostruct.* **2004**, *12*, 33–39.
9. Tan, K.; Lu, X. Ti_2C_{80} Is More Likely a Titanium Carbide Endohedral Metallofullerene $(Ti_2C_2)@C_{78}$. *Chem. Commun.* **2005**, 4444–4446.
10. Yumura, T.; Sato, Y.; Suenaga, K.; Iijima, S. Which Do Endohedral Ti_2C_{80} Metallofullerenes Prefer Energetically: $Ti_2@C_{80}$ or $Ti_2C_2@C_{78}$? A Theoretical Study. *J. Phys. Chem. B* **2005**, *109*, 20251–20255.
11. Sato, Y.; Yumura, T.; Suenaga, K.; Moribe, H.; Nishide, D.; Ishida, M.; Shinohara, H.; Iijima, S. Direct Imaging of Intracage Structure in Titanium-Carbide Endohedral Metallofullerene. *Phys. Rev. B* **2006**, *73*, 193401.
12. Popov, A. A.; Dunsch, L. Hindered Cluster Rotation and ^{45}Sc Hyperfine Splitting Constant in Distonoid Anion Radical $Sc_3N@C_{80}$, and Spatial Spin Charge Separation as a General Principle for Anions of Endohedral Fullerenes with Metal-Localized Lowest Unoccupied Molecular Orbitals. *J. Am. Chem. Soc.* **2008**, *130*, 17726–17742.
13. Guo, T.; Diener, M. D.; Chai, Y.; Alford, M. J.; Haufler, R. E.; McClure, S. M.; Ohno, T.; Weaver, J. H.; Scuseria, G. E.; Smalley, R. E. Uranium Stabilization of C_{28}: A Tetravalent Fullerene. *Science* **1992**, *257*, 1661–1664.
14. Dunlap, B. I.; Haberlen, O. D.; Rosch, N. Asymmetric Localization of Titanium in C_{28}. *J. Phys. Chem.* **1992**, *96*, 9095–9097.
15. Stevenson, S.; Rice, G.; Glass, T.; Harich, K.; Cromer, F.; Jordan, M. R.; Craft, J.; Hadju, E.; Bible, R.; Olmstead, M. M.; Maitra, K.; Fisher, A. J.; Balch, A. L.; Dorn, H. C. Small-Bandgap Endohedral Metallofullerenes in High Yield and Purity. *Nature* **1999**, *401*, 55–57.
16. Dunsch, L.; Yang, S. F. Endohedral Clusterfullerenes: Playing with Cluster and Cage Sizes. *Phys. Chem. Chem. Phys.* **2007**, *9*, 3067–3081.
17. Olmstead, M. H.; de Bettencourt-Dias, A.; Duchamp, J. C.; Stevenson, S.; Marciu, D.; Dorn, H. C.; Balch, A. L. Isolation and Structural Characterization of the Endohedral Fullerene $Sc_3N@C_{78}$. *Angew. Chem., Int. Ed.* **2001**, *40*, 1223–1225.
18. Olmstead, M. M.; Lee, H. M.; Duchamp, J. C.; Stevenson, S.; Marciu, D.; Dorn, H. C.; Balch, A. L. $Sc_3N@C_{68}$: Folded Pentalene Coordination in an Endohedral Fullerene That Does Not Obey the Isolated Pentagon Rule. *Angew. Chem., Int. Ed.* **2003**, *42*, 900–903.
19. Stevenson, S.; Fowler, P. W.; Heine, T.; Duchamp, J. C.; Rice, G.; Glass, T.; Harich, K.; Hajdu, E.; Bible, R.; Dorn, H. C. Materials Science: A Stable Non-Classical Metallofullerene Family. *Nature* **2000**, *408*, 427–428.
20. Krause, M.; Dunsch, L. Isolation and Characterisation of Two $Sc_3N@C_{80}$ Isomers. *ChemPhysChem* **2004**, *5*, 1445–1449.
21. Yang, S. F.; Kalbac, M.; Popov, A.; Dunsch, L. A Facile Route to the Non-IPR Fullerene $Sc_3N@C_{68}$: Synthesis, Spectroscopic Characterization, and Density Functional Theory Computations (IPR = Isolated Pentagon Rule). *Chem.—Eur. J.* **2006**, *12*, 7856–7863.
22. Yang, S. F.; Popov, A. A.; Dunsch, L. Violating the Isolated Pentagon Rule (IPR): The Endohedral Non-IPR Cage of $Sc_3N@C_{70}$. *Angew. Chem., Int. Ed.* **2007**, *46*, 1256–1259.
23. Dunsch, L.; Krause, M.; Noack, J.; Georgi, P. Endohedral Nitride Cluster Fullerenes: Formation and Spectroscopic Analysis of $L_{3-x}M_xN@C_{2n}$ ($0 \leq x \leq 3$; $n = 39, 40$). *J. Phys. Chem. Solids* **2004**, *65*, 309–315.
24. Krause, M.; Wong, J.; Dunsch, L. Expanding the World of Endohedral Fullerenes: The $Tm_3N@C_{2n}$ ($39 \leq n \leq 43$) Clusterfullerene Family. *Chem.—Eur. J.* **2005**, *11*, 706–711.
25. Yang, S. F.; Dunsch, L. A Large Family of Dysprosium-Based Trimetallic Nitride Endohedral Fullerenes: $Dy_3N@C_{2n}$ ($39 \leq n \leq 44$). *J. Phys. Chem. B* **2005**, *109*, 12320–12328.
26. Beavers, C. M.; Zuo, T. M.; Duchamp, J. C.; Harich, K.; Dorn, H. C.; Olmstead, M. M.; Balch, A. L. $Tb_3N@C_{84}$: An Improbable, Egg-Shaped Endohedral Fullerene That Violates the Isolated Pentagon Rule. *J. Am. Chem. Soc.* **2006**, *128*, 11352–11353.
27. Zuo, T.; Walker, K.; Olmstead, M. M.; Melin, F.; Holloway, B. C.; Echegoyen, L.; Dorn, H. C.; Chaur, M. N.; Chancellor, C. J.; Beavers, C. M.; Balch, A. L.; Athans, A. J. New Egg-Shaped Fullerenes: Non-Isolated Pentagon Structures of $Tm_3N@C_s(51365)-C_{84}$ and $Gd_3N@C_s(51365)-C_{84}$. *Chem. Commun.* **2008**, 1067–1069.
28. Zuo, T. M.; Beavers, C. M.; Duchamp, J. C.; Campbell, A.; Dorn, H. C.; Olmstead, M. M.; Balch, A. L. Isolation and Structural Characterization of a Family of Endohedral Fullerenes Including the Large, Chiral Cage Fullerenes $Tb_3N@C_{88}$ and $Tb_3N@C_{86}$ as Well as the I_h and D_{5h} Isomers of $Tb_3N@C_{80}$. *J. Am. Chem. Soc.* **2007**, *129*, 2035–2043.
29. Melin, F.; Chaur, M. N.; Engmann, S.; Elliott, B.; Kumbhar, A.; Athans, A. J.; Echegoyen, L. The Large $Nd_3N@C_{2n}$ ($40 \leq 2n \leq 49$) Cluster Fullerene Family: Preferential Templating of a C_{88} Cage by a Trimetallic Nitride Cluster. *Angew. Chem., Int. Ed.* **2007**, *46*, 9032–9035.
30. Chaur, M. N.; Melin, F.; Elliott, B.; Athans, A. J.; Walker, K.; Holloway, B. C.; Echegoyen, L. $Gd_3N@C_{2n}$ ($n = 40, 42,$ and 44): Remarkably Low HOMO–LUMO Gap and Unusual Electrochemical Reversibility of $Gd_3N@C_{88}$. *J. Am. Chem. Soc.* **2007**, *129*, 14826–14829.
31. Chaur, M. N.; Melin, F.; Ashby, J.; Kumbhar, A.; Rao, A. M.; Echegoyen, L. Lanthanum Nitride Endohedral Fullerenes $La_3N@C_{2n}$ ($43 < n < 55$): Preferential Formation of $La_3N@C_{96}$. *Chem.—Eur. J.* **2008**, *14*, 8213–8219.
32. Chaur, M. N.; Melin, F.; Elliott, B.; Kumbhar, A.; Athans, A. J.; Echegoyen, L. New $M_3N@C_{2n}$ Endohedral Metallofullerene Families (M = Nd, Pr, Ce; N = 40–53): Expanding the Preferential Templating of the C_{88} Cage and Approaching the C_{96} Cage. *Chem.—Eur. J.* **2008**, *14*, 4594–4599.
33. Krause, M.; Dunsch, L. Gadolinium Nitride Gd_3N in Carbon Cages: The Influence of Cluster Size and Bond Strength. *Angew. Chem., Int. Ed.* **2005**, *44*, 1557–1560.
34. Yang, S. F.; Troyanov, S. I.; Popov, A. A.; Krause, M.; Dunsch, L. Deviation from the Planarity—A Large Dy_3N Cluster Encapsulated in an I_h-C_{80} Cage: An X-Ray Crystallographic and Vibrational Spectroscopic Study. *J. Am. Chem. Soc.* **2006**, *128*, 16733–16739.
35. Stevenson, S.; Phillips, J. P.; Reid, J. E.; Olmstead, M. M.;

Rath, S. P.; Balch, A. L. Pyramidalization of Gd_3N inside a C_{80} Cage. The Synthesis and Structure of $Gd_3N@C_{80}$. *Chem. Commun.* **2004**, 2814–2815.

36. Chaur, M. N.; Valencia, R.; Rodriguez-Fortea, A.; Poblet, J. M.; Echegoyen, L. Trimetallic Nitride Endohedral Fullerenes: Experimental and Theoretical Evidence for the $M_3N^{6+}@C_{2n}^{6-}$ Model. *Angew. Chem., Int. Ed.* **2009**, *48*, 1425–1428.

37. Campanera, J. M.; Bo, C.; Olmstead, M. M.; Balch, A. L.; Poblet, J. M. Bonding within the Endohedral Fullerenes $Sc_3N@C_{78}$ and $Sc_3N@C_{80}$ as Determined by Density Functional Calculations and Reexamination of the Crystal Structure of $Sc_3N@C_{78} \cdot Co(Oep)1.5(C_6H_6)0.3(CHCl_3)$. *J. Phys. Chem. A* **2002**, *106*, 12356–12364.

38. Campanera, J. M.; Bo, C.; Poblet, J. M. General Rule for the Stabilization of Fullerene Cages Encapsulating Trimetallic Nitride Templates. *Angew. Chem., Int. Ed.* **2005**, *44*, 7230–7233.

39. Alvarez, L.; Pichler, T.; Georgi, P.; Schwieger, T.; Peisert, H.; Dunsch, L.; Hu, Z.; Knupfer, M.; Fink, J.; Bressler, P.; Mast, M.; Golden, M. S. Electronic Structure of Pristine and Intercalated $Sc_3N@C_{80}$ Metallofullerene. *Phys. Rev. B* **2002**, *66*, 035107.

40. Popov, A. A.; Dunsch, L. Structure, Stability, and Cluster-Cage Interactions in Nitride Clusterfullerenes $M_3N@C_{2n}$ (M = Sc, Y; $2n = 68-98$): A Density Functional Theory Study. *J. Am. Chem. Soc.* **2007**, *129*, 11835–11849.

41. Popov, A. A.; Dunsch, L. The Bonding Situation in Endohedral Metallofullerenes as Studied by Quantum Theory of Atoms in Molecules (QTAIM). *Chem.—Eur. J.* **2009**, *15*, 9707–9729.

42. Stevenson, S.; Chancellor, C.; Lee, H. M.; Olmstead, M. H.; Balch, A. L. Internal and External Factors in the Structural Organization in Cocrystals of the Mixed-Metal Endohedrals $(GdSc_2N@I_h-C_{80}, Gd_2ScN@I_h-C_{80},$ and $TbSc_2N@I_h-C_{80})$ and Nickel(II) Octaethylporphyrin. *Inorg. Chem.* **2008**, *47*, 1420–1427.

43. Yang, S. F.; Kalbac, M.; Popov, A.; Dunsch, L. Gadolinium-Based Mixed Metal Nitride Clusterfullerenes $Gd_xSc_{3-x}N@C_{80}$ (x = 1, 2). *ChemPhysChem* **2006**, *7*, 1990–1995.

44. Yang, S.; Popov, A. A.; Dunsch, L. The Role of an Asymmetric Nitride Cluster on a Fullerene Cage: The Non-IPR Endohedral $DySc_2N@C_{76}$. *J. Phys. Chem. B* **2007**, *111*, 13659–13663.

45. Yang, S. F.; Popov, A. A.; Dunsch, L. Large Mixed Metal Nitride Clusters Encapsulated in a Small Cage: The Confinement of the C_{68}-Based Clusterfullerenes. *Chem. Commun.* **2008**, 2885–2887.

46. Yang, S. F.; Popov, A. A.; Kalbac, M.; Dunsch, L. The Isomers of Gadolinium Scandium Nitride Clusterfullerenes $Gd_xSc_{3-x}N@C_{80}$ (x = 1, 2) and Their Influence on Cluster Structure. *Chem.—Eur. J.* **2008**, *14*, 2084–2092.

47. Yang, S.; Popov, A. A.; Chen, C.; Dunsch, L. Mixed Metal Nitride Clusterfullerenes in Cage Isomers: $Lu_xSc_{3-x}N@C_{80}$ (x = 1, 2) as Compared with $M_xSc_{3-x}N@C_{80}$ (M = Er, Dy, Gd, Nd). *J. Phys. Chem. C* **2009**, *113*, 7616–7623.

48. Olmstead, M. M.; de Bettencourt-Dias, A.; Duchamp, J. C.; Stevenson, S.; Dorn, H. C.; Balch, A. L. Isolation and Crystallographic Characterization of $ErSc_2N@C_{80}$: An Endohedral Fullerene Which Crystallizes with Remarkable Internal Order. *J. Am. Chem. Soc.* **2000**, *122*, 12220–12226.

49. Yang, S.; Popov, A. A.; Dunsch, L. Carbon Pyramidalization in Fullerene Cages Induced by the Endohedral Cluster: Non-Scandium Mixed Metal Nitride Clusterfullerenes. *Angew. Chem., Int. Ed.* **2008**, *47*, 8196–8200.

50. Yang, S.; Chen, C.; Popov, A.; Zhang, W.; Liu, F.; Dunsch, L. An Endohedral Titanium(III) in a Clusterfullerene: Putting a Non-Group-III Metal Nitride into the $C_{80}-I_h$ Fullerene Cage. *Chem. Commun.* **2009**, 6391–6393.

51. Elliott, B.; Yu, L.; Echegoyen, L. A Simple Isomeric Separation of D_{5h} and I_h $Sc_3N@C_{80}$ by Selective Chemical Oxidation. *J. Am. Chem. Soc.* **2005**, *127*, 10885–10888.

52. Suzuki, T.; Kikuchi, K.; Oguri, F.; Nakao, Y.; Suzuki, S.; Achiba, Y.; Yamamoto, K.; Funasaka, H.; Takahashi, T.

Electrochemical Properties of Fullerenolanthanides. *Tetrahedron* **1996**, *52*, 4973–4982.

53. Iiduka, Y.; Wakahara, T.; Nakahodo, T.; Tsuchiya, T.; Sakuraba, A.; Maeda, Y.; Akasaka, T.; Yoza, K.; Horn, E.; Kato, T.; Liu, M. T. H.; Mizorogi, N.; Kobayashi, K.; Nagase, S. Structural Determination of Metallofullerene Sc_3C_{82} Revisited: A Surprising Finding. *J. Am. Chem. Soc.* **2005**, *127*, 12500–12501.

54. Zhang, L.; Popov, A. A.; Yang, S.; Klod, S.; Rapta, P.; Dunsch, L. An Endohedral Redox Sytem in a Fullerene Cage: The Ce Based Mixed Cluster Fullerene $Lu_2CeN@C_{80}$. *Phys. Chem. Chem. Phys.* **2010**, (12), 7840–7847.

55. Jakes, P.; Dinse, K. P. Chemically Induced Spin Transfer to an Encased Molecular Cluster: An EPR Study of $Sc_3N@C_{80}$ Radical Anions. *J. Am. Chem. Soc.* **2001**, *123*, 8854–8855.

56. Popov, A. A.; Zhang, L.; Dunsch, L. A Pseudoatom in a Cage: Trimetallofullerene $Y_3@C_{80}$ Mimics $Y_3N@C_{80}$ with Nitrogen Substituted by a Pseudoatom. *ACS Nano* **2010**, *4*, 795–802.

57. Kobayashi, K.; Sano, Y.; Nagase, S. Theoretical Study of Endohedral Metallofullerenes: $Sc_{3-n}La_nN@C_{80}$ ($n = 0-3$). *J. Comput. Chem.* **2001**, *22*, 1353–1358.

58. Gan, L. H.; Yuan, R. Influence of Cluster Size on the Structures and Stability of Trimetallic Nitride Fullerenes $M_3N@C80$. *ChemPhysChem* **2006**, *7*, 1306–1310.

59. Heine, T.; Vietze, K.; Seifert, G. ^{13}C NMR Fingerprint Characterizes Long Time-Scale Structure of $Sc_3N@C_{80}$ Endohedral Fullerene. *Magn. Reson. Chem.* **2004**, *42*, S199–S201.

60. Valencia, R.; Rodriguez-Fortea, A.; Clotet, A.; de Graaf, C.; Chaur, M. N.; Echegoyen, L.; Poblet, J. M. Electronic Structure and Redox Properties of Metal Nitride Endohedral Fullerenes $M_3N@C_{2n}$ (M = Sc, Y, La, and Gd; $2n$ = 80, 84, 88, 92, 96). *Chem.—Eur. J.* **2009**, *15*, 10997–11009.

61. Wang, X. L.; Zuo, T. M.; Olmstead, M. M.; Duchamp, J. C.; Glass, T. E.; Cromer, F.; Balch, A. L.; Dorn, H. C. Preparation and Structure of $CeSc_2N@C_{80}$: An Icosahedral Carbon Cage Enclosing an Acentric $CeSc_2N$ Unit with Buried f Electron Spin. *J. Am. Chem. Soc.* **2006**, *128*, 8884–8889.

62. Ioffe, I. N.; Ievlev, A. S.; Boltalina, O. V.; Sidorov, L. N.; Dorn, H. C.; Stevenson, S.; Rice, G. Electron Affinity of Some Trimetallic Nitride and Conventional Metallofullerenes. *Int. J. Mass Spectrom.* **2002**, *213*, 183–189.

63. Krause, M.; Kuzmany, H.; Georgi, P.; Dunsch, L.; Vietze, K.; Seifert, G. Structure and Stability of Endohedral Fullerene $Sc_3N@C_{80}$: A Raman, Infrared, and Theoretical Analysis. *J. Chem. Phys.* **2001**, *115*, 6596–6605.

64. Hino, S.; Kato, M.; Yoshimura, D.; Moribe, H.; Umemoto, H.; Ito, Y.; Sugai, T.; Shinohara, H.; Otani, M.; Yoshimoto, Y.; Okada, S. Effect of Encapsulated Atoms on the Electronic Structure of the Fullerene Cage: A Case Study on $La_2@C_{78}$ and $Ti_2C_2@C_{78}$ via Ultraviolet Photoelectron Spectroscopy. *Phys. Rev. B* **2007**, *75*, 125418.

65. Bader, R. F. W. *Atoms in Molecules—A Quantum Theory*; Oxford University Press: Oxford, 1990.

66. Matta, C. F.; Boyd, R. J. *The Quantum Theory of Atoms in Molecules. From Solid State to DNA and Drug Design*; Wiley-VCH Verlag: Weinheim, 2007.

67. Perdew, J. P.; Burke, K.; Ernzerhof, M. *Phys. Rev. Lett.* **1996**, *77*, 3865–3868.

68. Laikov, D. N. Fast Evaluation of Density Functional Exchange-Correlation Terms Using the Expansion of the Density in Auxiliary Basis Sets. *Chem. Phys. Lett.* **1997**, *281*, 151–156.

69. Laikov, D. N.; Ustynyuk, Y. A. Priroda-04: A Quantum-Chemical Program Suite. New Possibilities in the Study of Molecular Systems with the Application of Parallel Computing. *Russ. Chem. Bull., Int. Ed.* **2004**, *54*, 820–826.

70. Granovsky, A. A. PC Gamess/Firefly, version 7.1.F; http://classic.chem.msu.su/gran/gamess/index.html, 2009.